ISSN 1087-6596, Glass Physics and Chemistry, 2016, Vol. 42, No. 1, pp. 20–26. © Pleiades Publishing, Ltd., 2016.

Effect of Feldspar Addition into Bioglass 45S5 Composition: Crystallization Kinetics and Thermal Transformation[1]

Franco Matias Stábile and Cristina Volzone

Centro de Tecnología de Recursos Minerales y Cerámica (CETMIC) (Technology Center of Mineral Resourses and Ceramic), CCT CONICET La Plata—CICPBA, Camino Centenario y 506, (1897) M.B. Gonnet, Provincia de Buenos Aires, Argentina

e-mail: mstabile@cetmic.unlp.edu.ar

Received December 18, 2015

Abstract—Thermal transformations of glasses with formulations derived from Bioglass 45S5 with Al_2O_3 (≤2.5 wt %) and K_2O additions through K-feldspar were studied. Crystallization kinetics and transformations were followed-up by X-ray diffraction and differential thermal analysis. The activation energy of crystallization of $Na_2CaSi_2O_6$ was found to be lower than that of Bioglass 45S5 for the prepared samples. This behavior was attributed to an increase in phase separation in glasses. Nevertheless, transformations shifted towards higher temperatures with addition of feldspar, due to a decrease in pre-exponential factor. Cell parameters evolved progressively with increasing temperature without any abrupt changes. Al_2O_3 and K_2O remained as a part of a residual glassy phase.

Keywords: glass, glass-ceramics, crystallization kinetics, differential thermal analysis, X-ray diffraction

DOI: 10.1134/S108765961601017X

INTRODUCTION

Bioglass is a biocompatible material which has the capability of bond to bone tissue. This property is reached thanks to a hydroxyapatite layer that is formed on the material surface when it is submerged in the body fluid. Bioglass 45S5 can formed a hydroxyapatite layer in a few hours [1, 2], which facilitates bone bonding, as well as being osteoconductive [3]. However, one of its main disadvantages is mechanical weakness and low fracture resistance making it undesirable for load bearing applications. In addition, its high dissolution rate does not match with bone tissue growth. A way to increase mechanical strength and at the same time to control the dissolution rate is through Al_2O_3 addition into the glass composition. However, 3 wt % of Al_2O_3 addition prevents bone bonding ability of Bioglass 45S5 [4–6]. Bioactive glass and glass-ceramics are generally produced using high purity raw materials. However, natural minerals could be incorporated, if strict compositions controls are take into account. Feldspar is one of the most broadly used mineral in glass industry to incorporate Al_2O_3. Nevertheless, no studies have been found regarding the use of feldspar as a raw material for bioactive glass-ceramics production.

More to know about the transformations that take place in the glass by heat treatment, it is necessary for the production of glass ceramic and related products like porous glass ceramics for tissue engineering applications [7–9]. In this sense, the objective of the present study was to produce two glasses with formulations derived from Bioglass 45S5 with Al_2O_3 and K_2O additions through very pure feldspar from a mining industry. At the same time, the effects of the incorporation of both oxides on thermal transformations of glasses were studied.

EXPERIMENTAL

Sample Preparation

Raw materials were reagent grade sodium carbonate, calcium carbonate, monobasic ammonium phosphate; and natural high purity quartz and potassium feldspar which were provided by an Argentinian mining company, whose compositions are listed in Table 1.

Feldspar addition was established according to the amount of aluminium, whose values were selected as 0.5 and 2.5 wt %, expressed as Al_2O_3. Consequently the incorporation of potassium from feldspar was fixed. The prepared samples were identified as B45Al5 and B45Al25, respectively. Amounts of phosphorous, calcium and silicon (expressed as oxides) were constants for all samples. Samples compositions (wt %) expressed as oxides are shown in Table 2.

The mixtures were previously treated at 900°C for decarbonation, melted at 1350°C in platinum crucible for 2 h, and then cast into cold distillate water (quenching) to obtain glass frits. Glasses were crushed to pass through 100 mesh.

[1] The article is published in the original.

Table 1. Chemical analyses of the natural raw materials (wt %)

Raw material	SiO_2	Al_2O_3	Na_2O	K_2O	CaO	Fe_2O_3	TiO_2
Feldspar	66.25	18.42	2.06	12.02	0.20	0.05	0.01
Quartz	99.33	0.49	0.06	0.10	0.00	0.01	0.00

Table 2. Nominal compositions of glasses (wt %)

Sample	Na_2O	CaO	SiO_2	P_2O_5	Al_2O_3	K_2O	Others
B45Al5	23.74	24.50	45.00	6.00	0.50	0.23	0.03
B45Al25	20.41	24.50	45.00	6.00	2.50	1.55	0.04

Differential Thermal Analysis

Thermal analyses were carried out by Netzsch STA 409 equipment at 5, 10, 15 and 20°C min^{-1} in air atmosphere with a flow rate of 50 mL min^{-1}. α-Al_2O_3 was used as reference material. Tests performed at 10°C min^{-1} were taken up to 1300°C.

The activation energy of crystallization was determined by Kissinger equation [10]:

$$\ln\left(\frac{\beta}{T_p^2}\right) = -\frac{E_c}{RT_p} + C, \quad (1)$$

where β is heating rate, T_p is the crystallization peak temperature, E_c is the activation energy for all the crystallization processand, C is a constant.

The Avrami exponent, which gives information about the mechanism of nucleation and crystal grow, was determined by the Ozawa's equation [11]:

$$-\ln(-\ln(1-\alpha)) = n\ln(\beta) + C, \quad (2)$$

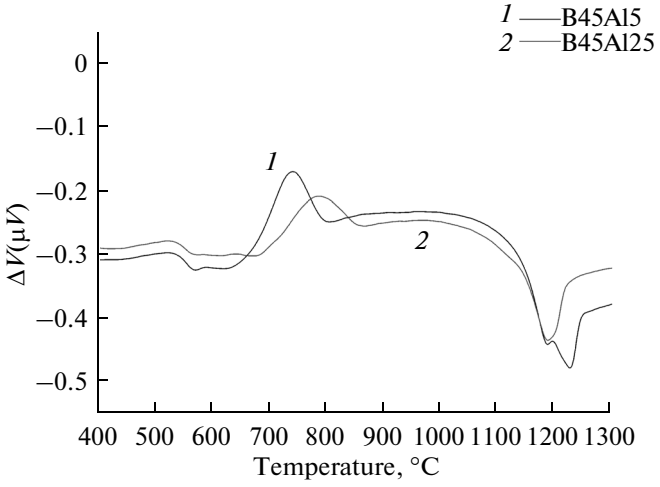

Fig. 1. Differential thermal analyses of B45Al5 and B45Al25 glasses performed at 10°C min^{-1}.

where α is the crystallized fraction determined as the normalized area under the DTA crystallization peak at a fixed temperature.

Heat Treatments

Thermal treatments were performed using an electrical furnace with a heating rate of 10°C min^{-1}. Samples were taken out from the furnace at different temperatures based on the performed thermal analyses at the same heating rate, and quenched to room temperature. The selected temperatures were 600, 700, 800, 900 and 1100°C.

X-ray Diffraction

Solids were characterized by X-ray diffraction (XRD) on Philips 3010 equipment using CuK_α-radiation at 40 kV and 35 mA, with a 0.04° (2θ) step, 2 s per step and Ni filter.

Fullprof software was used for phase quantification, cell parameters and apparent crystal size measurement.

RESULTS

Differential Thermal Analysis

DTA signal showed a significant difference between B45Al5 and B45Al25 crystallization and melting peaks.

Thermal analyses conducted at 10°C min^{-1} were used to compare glasses behaviors (Fig. 1). Both glasses showed a glass transition temperature around 550°C. A second glass transition temperature was found around 600 and 650°C for B45Al5 and B45Al25, respectively. Crystallization peak was shifted to a higher temperature for sample B45Al25. The temperature of melting (T_m) of B45Al5 was 1225°C, while for B45Al25 was 1186°C. The endothermic effect of melting in to B45Al5 consisted in two clearly marked peaks, while only one peak was distinguishable in to B45Al25, besides the melting process was completed at a lower temperature.

The temperature of crystallization peak (T_p) for each heating rate for B45Al5 and B45Al25 are shown in Table 3.

Kissinger plot was made from non-isothermal DTA data (Fig. 2). The slope of $-\ln\left(\frac{\beta}{T_p^2}\right)$ vs $\frac{1}{RT_p}$ linear regression (Eq. 1) yielded an activation energy of 246 (±4) and 234 (±28) kJ/mol for B45Al5 and B45Al25, respectively.

The Avrami exponent (n) calculated by the Ozawa method (Eq. 2) in the temperature range where the activation energy was evaluated. The Value of n varied between 1.25–1.09 and 0.98–0.95 for B45Al5 and B45Al25, respectively (Fig. 3). These values confirmed surface crystallization mechanism. Besides, due to the mechanism of surface crystallization, Kissinger equation could be simplified and the pre-exponential factor could be calculated from the constant C. The calculated factors were 3.05×10^{10} s^{-1} for B45Al5 and 2.03×10^{9} s^{-1} for B45Al25.

X-ray Diffraction

Figure 4 shows the XRD patterns of B45Al5 and B45Al25 glasses. The broad band indicated that both materials had no long range order, which confirmed that both samples were glasses. Moreover, two broad overlapped halos/bands were visible for the two diffractograms; the bigger sited at around 30°(2θ) and the other at around 20°(2θ).

B45Al5 glass showed no change after thermal treatment up to 600°C, as the X-ray pattern did not change from the original glass (Fig. 5). Some diffraction peaks had appeared when the thermal treatment was stopped at 700°C.

Table 3. T_p (°C) as function of heating rate

Sample	5°C min^{-1}	10°C min^{-1}	15°C min^{-1}	20°C min^{-1}
B45Al5	712	733	747	756
B45Al25	755	777	788	807

An increase of diffraction peaks intensities was observed after temperature evolution up to 800°C due to crystallization. Heat treatment up to 900°C did not show an appreciable change in peaks intensities, nevertheless, peaks were more defined because of the crystal growth that reduced their widths. The final thermal treatment enabled an easy identification of the developed crystal phases. X-ray pattern of the treated sample at 1100°C matched with $Na_2CaSi_2O_6$ (PDF 01-077-2189) and $NaCaPO_4$ (PDF 01-076-1456). As can be seen in Fig. 5, $Na_2CaSi_2O_6$ was the primary developed phase, which had started to crystallize at 700°C. Then, $NaCaPO_4$ peaks appeared at 900°C.

Thermal evolution of B45Al25 glass (Fig. 6) was similar than that of B45Al5. Crystallization advance was lower than B45Al5 at 700°C. The same crystalline phases were found within the final thermal treatment, but the relative amounts of each phase were somewhat different.

Crystalline phase quantifications were conducted on the 1100°C heat-treated samples. The results are listed in Table 4.

As Rietveld refinement can only quantify crystalline phases, the amorphous content remains

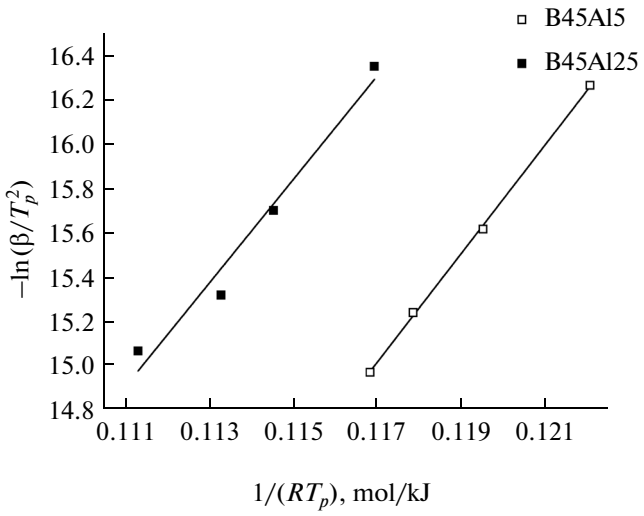

Fig. 2. Kissinger plot for activation energy of crystallization determination.

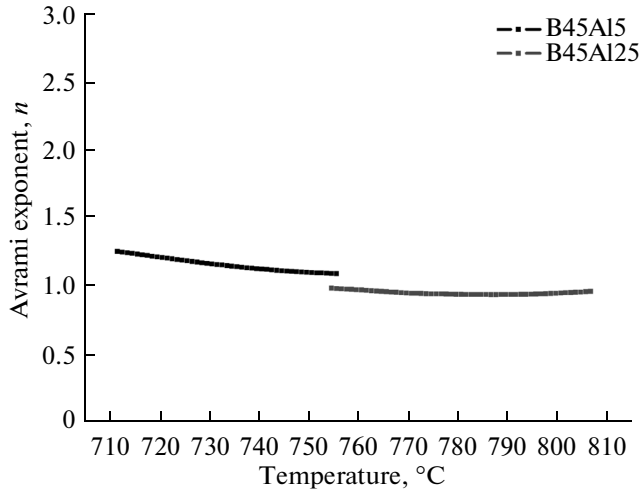

Fig. 3. Avrami exponent calculated by the Ozawa equation for B45Al5 and B45Al25 glasses.

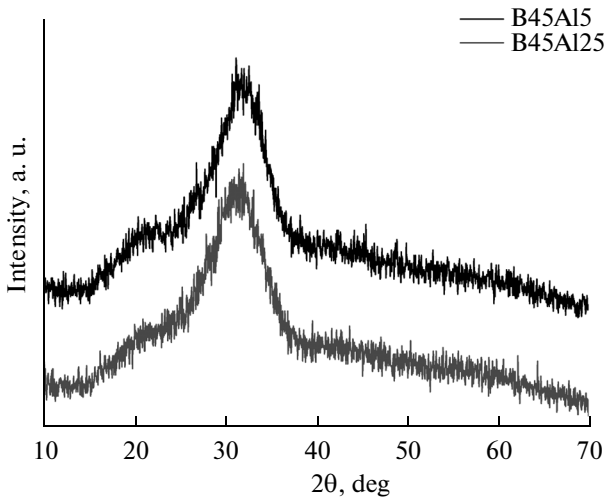

Fig. 4. X-ray diffractograms of as-received B45Al5 and B45Al25 glasses.

unknown. It is possible to calculate theoretical amounts of each crystalline phase taking into account the nominal composition of the glass sample and the nominal composition of each present crystalline phase. When the minor components are depleted in relation to the formed crystalline phases, all of the excess components remain as a part of an amorphous phase. In this way, the theoretical calculations were done (Table 5).

On the basis of the calculated amount of crystalline phases, it was possible to calculate the theoretical Rietveld quantification too (Table 5), so as to compare the experimental results with theoretical ones.

Comparison of the estimated a good agreement between theoretical calculations and experimental results. The temperature evolutions of sodium calcium silicate ($Na_2CaSi_2O_6$, rhombohedral) cell parameters were determined by Rietveld refinement (Figs. 7 and 8). The same tendency was found in both samples; *a* and *b* cell parameters decreased with temperature (Fig. 7), while *c* increased (Fig. 8). Parameters *a* and *b* were somewhat higher in B45A15 than in B45A125 at 700 and 800°C, but they reached approximately the same value at 900°C and higher temperatures. Cell parameter *c* was only found to be different at 700°C, while there was no difference at higher temperatures.

Apparent crystal sizes were calculated by means of the Williamson-Hall model, taking into account the inherent peaks width attributed to the instrument resolution. Crystals were found to grow at increasing temperatures in both samples (Fig. 9), as it was expected. Crystal size in B45Al5 was higher than B45Al25 at 700°C. Temperature increase up to 800°C provoked that crystals size of B45Al25 surpassed that of B45Al5, while at 900°C B45AL5 trended to increase more.

DISCUSSION

Thermal analysis of glasses showed some differences in their evolutions as a function of temperature. The activation energies of crystallization of the primary crystalline phase were of the same order for both samples (246 and 234 kJ/mol), at the time that surface crystallization mechanism was predominant as revealed by the Avrami exponent. It is known that Bioglass 45S5 suffers bulk crystallization [12]. However, the mechanism of surface crystallization is activated

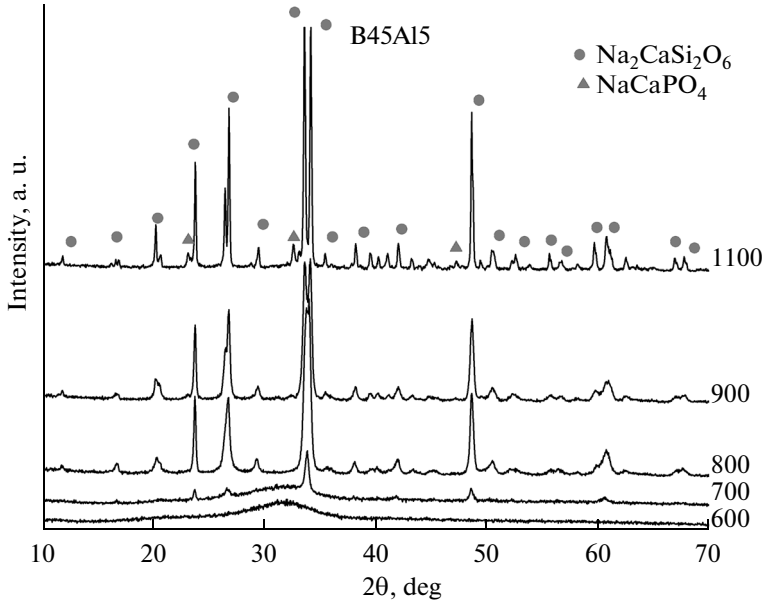

Fig. 5. X-ray difractograms of heat treated B45Al5 glass up to 600, 700, 800, 900, and 1100°C.

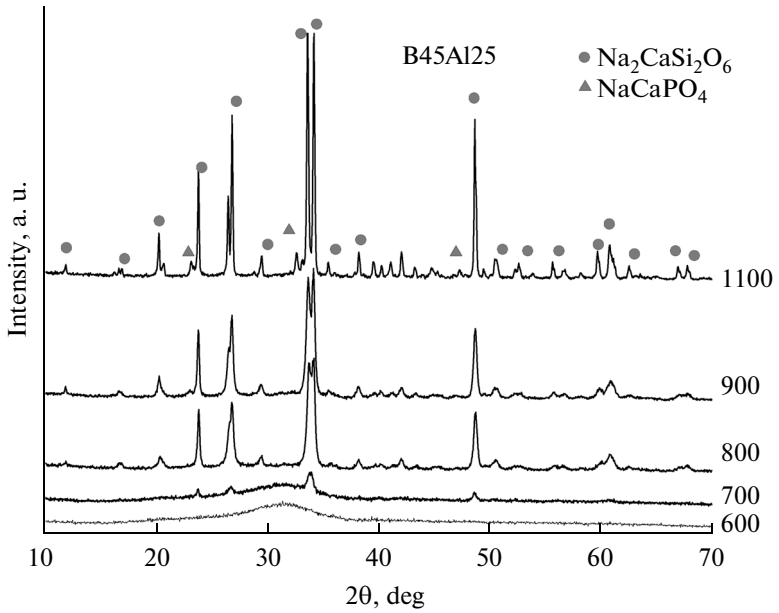

Fig. 6. X-ray difractograms of heat treated B45Al25 glass up to 600, 700, 800, 900, and 1100°C.

when Bioglass is ground to small particle size [13]. Although the activation energies were similar, temperatures range at which crystallization occurs was lower for B45Al5 with respect to B45Al25. Change in crystallization kinetics was attributed to a lower value, in one order of magnitude, of the pre-exponential factor for B45Al25 crystallization.

Activation energy of crystallization of Bioglass 45S5 was found in the range 310–350 kJ/mol [13–16]. According to [15], Bioglass 45S5 undergoes a phase separation in a silicate-rich and a phosphate-rich phases after a thermal treatment above 580°C [15]. It is known that when two high valence ions, namely Si^{4+} and P^{5+}, are present simultaneously in a glass, each ion tends to create a separate phase [17].

The phosphate phase could act as heterogeneous nucleation site for crystallization to take place; and it is the main reason why Bioglass 45S5 is prone to devitrification [18]. Diffractograms of both amorphous solids characterized in this study showed a shoulder close to $2\theta = 20°$. Besides, as shown in Fig. 1, a second glass transition can be observed at the approximate temperature of 600 and 650°C for B45A145 and B45A125 respectively. This may indicate that glasses phase separated, which is a possible reason for the activation energy of crystallization reduction compared to Bioglass. It is possible that the mentioned above reduction of energy is related to the fact that the addition of the aluminum through K-feldspar would improve phase separation, which would increase the number of crystal nuclei. Aluminum incorporation could play an important role on phosphate rich phase separation. The P^{5+} ion will locally charge compensate for the charge deficient Al^{3+} ion [19] and some of PO_4 tetrahedra in the glass are probably connected with AlO_4 tetrahedra. In addition, aluminum and potassium incorporation at the expense of sodium increases the network connectivity, leading to an increase in the glass viscosity, which slows down the crystallization kinetics. Therefore, according to the results, the viscosity was the factor that governed the kinetics of crystallization.

Table 4. Crystalline phase quantification and goodness of fit from Rietveld refinements of 1100°C treated samples

Samples	$Na_2CaSi_2O_6$	$NaCaPO_4$	Chi ^{2}
B45Al5	81.1 (3.1)	13.9 (1.0)	3.43
B45Al25	81.5 (6.3)	18.5 (2.2)	4.12

It was thought that both aluminum and potassium were incorporated within a residual amorphous phase according to the crystalline phases quantities that can form after complete crystallization; and due to the fact that there was no clear evidence that aluminum and potassium were incorporated into any of the crystalline phases. The amount of the non-crystallized glass remains estimated on the basis of the computation and comparison to the Rietveld refinements results indicated a higher residual glassy phase amount for B45A125. Hence it is reasonable to think that in this case viscous flow was enhanced, thus sintering was favored. A major quantity of residual glassy phase is the cause by which fusion was early completed, due to the fact that a greater amount of liquid phase could help to improve dissolution of the crystallized phases. On the other hand, the shift ofmelting temperature could be attributed to the formation of Al–O bonds,

Table 5. Theoretical amounts of crystalline and amorphous phases and theoretical Rietveld quantification of crystalline phases

Sample	$Na_2CaSi_2O_6$	$NaCaPO_4$	Amorphous phase
B45Al5 theoretical	81.2	13.4	5.5
B45Al5 theoretical Rietveld	85.9	14.1	–
B45Al25 theoretical	68.4	13.4	18.2
B45Al25 theoretical Rietveld	83.7	16.3	–

which are weaker than Si–O bonds. The Al^{3+} ion can replace Si^{4+} ion in the silicate network as they have very similar ionic radius. However, the replacement of silicon by aluminum ions is associated with a reduction of the number of bridging oxygen, since aluminum atoms are in part six-fold coordinated, and aluminum can act as network modifier producing nonbridging oxygen atoms. Thus, the silicate network is weakened by breaking its continuity, leading to a decrease in the melting point temperature (T_m) [20].

The evolution of cell parameters of the primary phase presented a different dynamics with regard to Bioglass 45S5. The thermal evolution of the cell parameter *a* for B45Al5 and B45Al25 took greater values than those found for the Bioglass [15], while the *c* parameter was lower in both samples regarding Bioglass. Nevertheless, both studied samples reach almost the same values of lattice parameters with thermal treatments higher than 900°C (Figs. 7 and 8). Differences in lattice dynamics between B45Al5 and B45Al25 would appear due to crystallization kinetics. Main differences are in the range 700–800°C (Fig. 1). At 700°C B45Al5 has begun to crystallize, while B45Al25 still not. At 800°C, B45Al5 crystallization has ended, whereas B45Al25 was completed at around 50%. It has been found that the primary phase that crystallizes into Bioglass has P^{5+} ion in solid solution. In addition, phosphorus suffers a rapid departure from the silicate phase around 800°C, stated by a sudden change in the value of the cell parameter *c*, to then take place into silicorhenanite [15]. The same behavior was observed for the studied; however both solids showed a smooth and continuous change of the parameters *a* (*b*) and *c* in the entire temperature range studied, which means that phosphorus output was controlled. In addition the crystalline phosphate phase was not detected at least up to 900°C, what corresponds not to the silicorhenanite ($Na_2Ca_4(PO_4)_2SiO_4$), but to the buchwaldite ($NaCaPO_4$) (PDF 01-076-1456). Phosphorus requirement to form buchwaltite at around 900°C were completed without need of a high rate departure from the silicate crystalline phase.

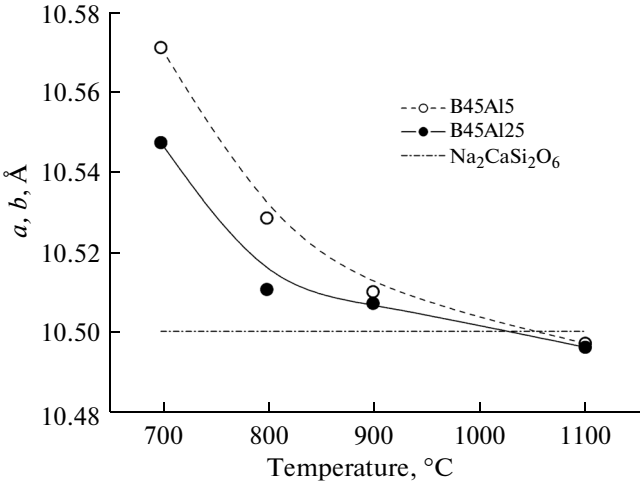

Fig. 7. Temperature evolution of $Na_2CaSi_2O_6$ cell parameter *a* for B45Al5 and B45Al25 samples compared with cell parameter *a* and *b* of PDF 01-077-2189.

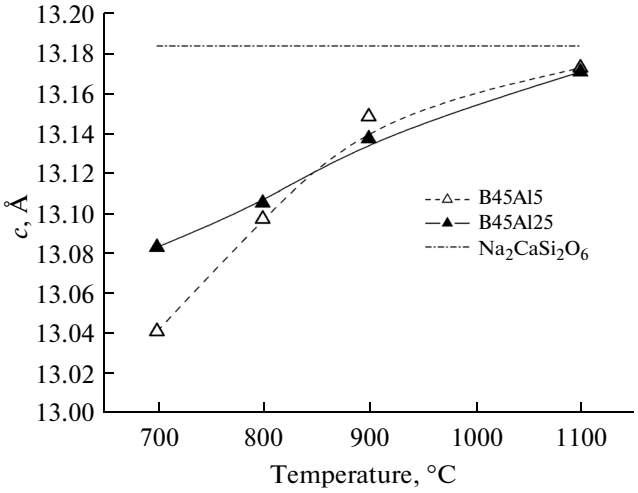

Fig. 8. Temperature evolution of $Na_2CaSi_2O_6$ cell parameter *c* for B45Al5 and B45Al25 samples compared with cell parameter *c* of PDF 01-077-2189.

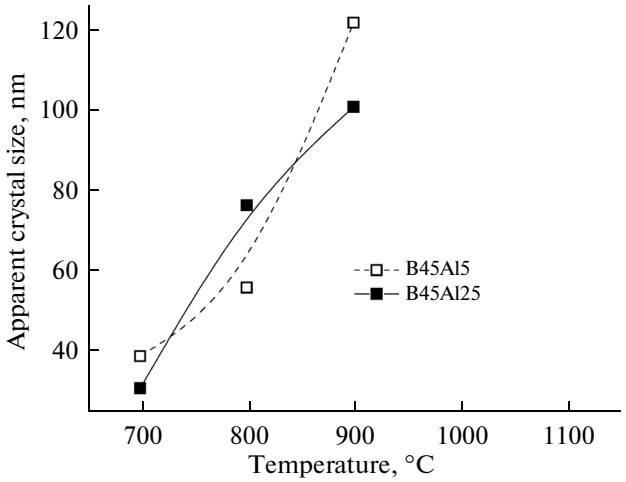

Fig. 9. Thermal evolution of the apparent crystal sizes of $Na_2CaSi_2O_6$.

CONCLUSIONS

Different additions of Al_2O_3 and K_2O incorporated through K-feldspar, to replace Na_2O of the bioglass composition, resulted in transformation kinetics and structural evolution changes of sodium calcium silicate ($Na_2CaSi_2O_6$).

Crystallizations were shifted to higher temperatures with feldspar addition; while the activation energies were lower than that of Bioglass 45S5.

Al_2O_3 and K_2O were not incorporated into the developed crystalline phases and they were thought to remain as a part of a residual glassy phase. On the other hand, they also led to a different cell parameters evolution of the major crystalline phase ($Na_2CaSi_2O_6$), due to the difference incrystallization kinetics. Phosphorus departure was controlled in the entire range of studied temperatures, which did that lattice parameters evolutions were continuous, without abrupt changes.

ACKNOWLEDGMENTS

The authors thank to CONICET (National Council of Scientific and Technical Research) for its financial support (PIP 0248) and Jose Ortiga for his important technical assistance.

REFERENCES

1. Filgueiras, M.R.T., La Torre, G., and Hench, L.L., Solution effects on the surface reactions of three bioactive glass compositions, *J. Biomed. Mater. Res.,* 1993, vol. 27, no. 12, pp. 1485–1493.
2. Peitl, O., Zanotto, E.D., and Hench, L.L., Highly bioactive P_2O_5–Na_2O–CaO–SiO_2 glass–ceramics, *J. Non-Cryst. Solids,* 2001, vol. 292, nos. 1–3, pp. 115–126.
3. Heikkilä, J.T., Aho, A.J., Yli-Urpo, A., Andersson, Ö.H., Aho, H.J., and Happonen, R.P., Bioactive glass versus hydroxylapatite in reconstruction of osteochondral defects in the rabbit, *Acta Orthop.,* 1993, vol. 64, no. 6, pp. 678–682.
4. Hench, L.L., Bioceramics: From concept to clinic, *J. Am. Ceram. Soc.,* 1991, vol. 74, no. 7, pp. 1487–1510.
5. Hench, L.L. and Paschall, H., Direct chemical bond of bioactive glass–ceramic materials to bone and muscle, *J. Biomed. Mater. Res.,* 1973, vol. 7, no. 3, pp. 25–42.
6. Andersson, Ö., Liu, G., Karlsson, K., Niemi, L., Miettinen, J., and Juhanoja, J., In vivo behaviour of glasses in the SiO_2–Na_2O–CaO–P_2O_5–Al_2O_3–B_2O_3 system, *J. Mater. Sci.: Mater. Med.,* 1990, vol. 1, no. 4, pp. 219–227.
7. Chen, Q., Mohn, D., and Stark, W.J., Optimization of Bioglass® scaffold fabrication process, *J. Am. Ceram. Soc.,* 2011, vol. 94, no. 12, pp. 4184–4190.
8. Jones, J.R., Ehrenfried, L.M., and Hench, L.L., Optimising bioactive glass scaffolds for bone tissue engineering, *Biomaterials,* 2006, vol. 27, no. 7, pp. 964–973.
9. Chen, Q.Z., Thompson, I.D., and Boccaccini, A.R., 45S5 Bioglass®-derived glass–ceramic scaffolds for bone tissue engineering, *Biomaterials,* 2006, vol. 27, no. 11, pp. 2414–2425.
10. Blaine, R.L. and Kissinger, H.E., Homer Kissinger and the Kissinger equation, *Thermochim. Acta,* 2012, vol. 540, pp. 1–6.
11. Ozawa, T., Kinetic analysis of derivative curves in thermal analysis, *J. Therm. Anal.,* 1970, vol. 2, no. 3, pp. 301–324.
12. Arstila, H., Vedel, E., Hupa, L., and Hupa, M., Factors affecting crystallization of bioactive glasses, *J. Eur. Ceram. Soc.,* 2007, vol. 27, nos. 2–3, pp. 1543–1546.
13. Massera, J., Fagerlund, S., Hupa, L., and Hupa, M., Crystallization mechanism of the bioactive glasses, 45S5 and S53P4, *J. Am. Ceram. Soc.,* 2012, vol. 95, no. 2, pp. 607–613.
14. Clupper, D.C. and Hench, L.L., Crystallization kinetics of tape cast bioactive glass 45S5, *J. Non-Cryst. Solids,* 2003, vol. 318, nos. 1–2, pp. 43–48.
15. Lefebvre, L., Chevalier, J., Gremillard, L., Zenati, R., Thollet, G., Bernache-Assolant, D., and Govin, A., Structural transformations of bioactive glass 45S5 with thermal treatments, *Acta Mater.,* 2007, vol. 55, no. 10, pp. 3305–3313.
16. Bretcanu, O., Chatzistavrou, X., Paraskevopoulos, K., Conradt, R., Thompson, I., and Boccaccini, A.R., Sintering and crystallisation of 45S5 Bioglass® powder, *J. Eur. Ceram. Soc.,* 2009, vol. 29, no. 16, pp. 3299–3306.
17. Doremus, R.H. and Sigel, Jr., G.H., *Glass Science,* 2nd ed., New York: Wiley, 1994.
18. Bellucci, D., Cannillo, V., and Sola, A., An overview of the effects of thermal processing on bioactive glasses, *Sci. Sintering,* 2010, vol. 42, no. 3, pp. 307–320.
19. Hill, R.G., Stamboulis, A., Law, R.V., Clifford, A., Towler, M.R., and Crowley, C., The influence of strontium substitution in fluorapatite glasses and glass–ceramics, *J. Non-Cryst. Solids,* 2004, vol. 336, no. 3, pp. 223–229.
20. Chatzistavrou, X., Chrissafis, K., Polychroniadis, E., Kontonasaki, E., Koidis, P., and Paraskevopoulos, K.M., Inducing bioactivity in dental porcelain through Bioglass®: Changes in thermal behaviour, *J. Therm. Anal. Calorim.,* 2006, vol. 86, no. 1, pp. 255–259.